Article

Cell Reports

Vegfc Regulates Bipotential Precursor Division and Prox1 Expression to Promote Lymphatic Identity in Zebrafish

Graphical Abstract

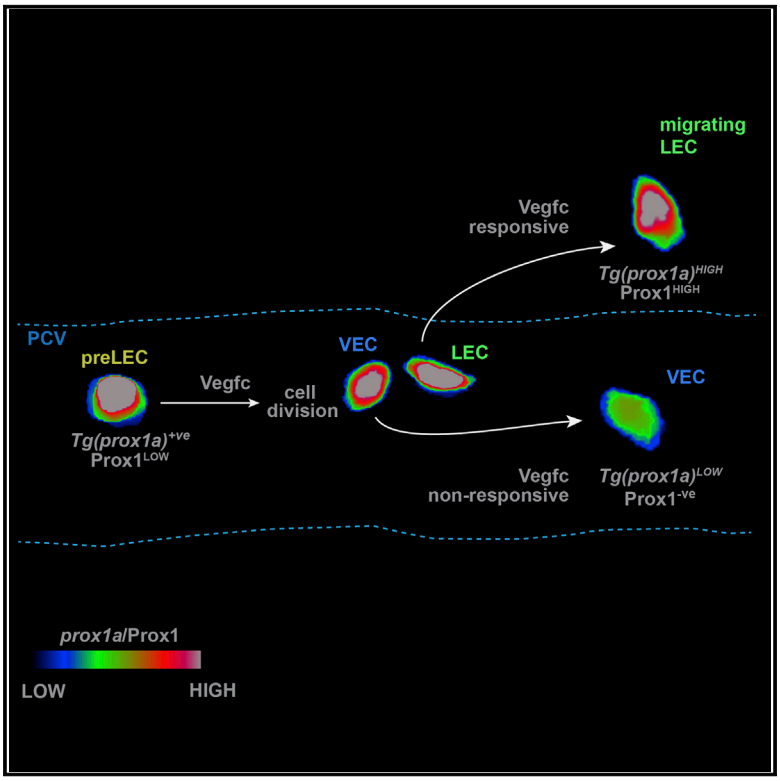

Authors

Katarzyna Koltowska,
Anne Karine Lagendijk,
Cathy Pichol-Thievend, ..., Elke A. Ober,
Alpha S. Yap, Benjamin M. Hogan

Correspondence

b.hogan@imb.uq.edu.au

In Brief

Using live imaging, Koltowska and Lagendijk et al. identify bipotential Prox1-expressing precursor cells that divide to generate daughter cells with distinct identities. Following Vegfc-driven cell division, a venous daughter cell remains in the vein and a lymphatic daughter cell leaves, a process by which one vascular lineage derives from another.

Highlights

- Prox1 expression initiates in the zebrafish vein before secondary angiogenesis
- Prox1 is essential for lymphangiogenesis in zebrafish
- Bipotential precursors divide to generate venous and lymphatic endothelial cells
- Vegfc concomitantly drives bipotential precursor division and Prox1 expression

Koltowska et al., 2015, Cell Reports *13*, 1828–1841
December 1, 2015
http://dx.doi.org/10.1016/j.celrep.2015.10.055

OPEN ACCESS
CellPress

Cell Reports
Article

Vegfc Regulates Bipotential Precursor Division and Prox1 Expression to Promote Lymphatic Identity in Zebrafish

Katarzyna Koltowska,[1,5] Anne Karine Lagendijk,[1,2,5] Cathy Pichol-Thievend,[1] Johanna C. Fischer,[4] Mathias Francois,[1] Elke A. Ober,[3,4] Alpha S. Yap,[2] and Benjamin M. Hogan[1,*]
[1]Division of Genomics of Development and Disease
[2]Division of Cell Biology and Molecular Medicine
Institute for Molecular Bioscience, The University of Queensland, St Lucia, QLD 4072, Australia
[3]DanStem, University of Copenhagen, Blegdamsvej 3B, 2200 Copenhagen N, Denmark
[4]Developmental Biology, MRC National Institute for Medical Research, London NW7 1AA, UK
[5]Co-first author
*Correspondence: b.hogan@imb.uq.edu.au
http://dx.doi.org/10.1016/j.celrep.2015.10.055

SUMMARY

Lymphatic vessels arise chiefly from preexisting embryonic veins. Genetic regulators of lymphatic fate are known, but how dynamic cellular changes contribute during the acquisition of lymphatic identity is not understood. We report the visualization of zebrafish lymphatic precursor cell dynamics during fate restriction. In the cardinal vein, cellular commitment is linked with the division of bipotential Prox1-positive precursor cells, which occurs immediately prior to sprouting angiogenesis. Following precursor division, identities are established asymmetrically in daughter cells; one daughter cell becomes lymphatic and progressively upregulates Prox1, and the other downregulates Prox1 and remains in the vein. Vegfc drives cell division and Prox1 expression in lymphatic daughter cells, coupling signaling dynamics with daughter cell fate restriction and precursor division.

INTRODUCTION

To form functioning tissues, individual precursor cells acquire distinct identities and differentiate under the influence of cell-cell signaling, growth factor signaling, and mechanical forces. In the vasculature, lymphatic endothelial cells (LECs) arise primarily from the preexisting venous endothelial cells (VECs) of the early embryo by spouting from the cardinal vein and subsequently migrating to colonize embryonic tissues (Sabin, 1902; Srinivasan et al., 2007). Overall, the developmental origins of LECs and the factors promoting lymphangiogenesis are largely conserved between vertebrates (reviewed in Koltowska et al., 2013). However, recent findings have suggested diversity in the origins of LECs in some vascular beds (Klotz et al., 2015; Mahadevan et al., 2014; Martinez-Corral et al., 2015; Stanczuk et al., 2015).

In mice, Prospero-related homeobox domain 1 (PROX1) is expressed in the dorsal wall of the cardinal vein (CV) from embryonic day 9.5 (E9.5) and is thought to mark specified LECs (Wigle et al., 2002; Wigle and Oliver, 1999). PROX1 is essential for lymphatic vessel development in mice and has the capability to direct LEC fate when overexpressed in endothelial cells (ECs) (Hong et al., 2002; Kim et al., 2010; Wigle et al., 2002; Wigle and Oliver, 1999; Yang et al., 2012). Once LECs induce PROX1 expression, these cells vacate the CV, sprouting in response to signaling induced by VEGFC, through its receptor VEGFR3 (Hägerling et al., 2013; Karkkainen et al., 2004).

Zebrafish secondary angiogenic sprouts emerge from the posterior CV (PCV) from 36 hr postfertilization (hpf) and generate either venous intersegmental vessels (vISVs) or alternating lymphatic precursors, which have sprouted to the horizontal myoseptum (HM) by 48 hpf (Bussmann et al., 2010; Hogan et al., 2009a; Isogai et al., 2009; Yaniv et al., 2006). This process depends on Vegfc, Ccbe1, and Vegfr3 (Flt4) signaling as in mice (Hogan et al., 2009a, 2009b; Villefranc et al., 2013). However, the developmental stage when lymphatic precursors become fate restricted in zebrafish has been contentious (Geudens et al., 2010; Koltowska et al., 2013; van Impel et al., 2014). Recent observations have suggested that LECs may arise well in advance of secondary sprouting from the PCV, from a pool of ventral PCV angioblasts from 24 hpf (Nicenboim et al., 2015). These ventral angioblasts are multipotent, generating arterial ECs (AECs), VECs (in the sub-intestinal vasculature), and secondary sprouts (Nicenboim et al., 2015). However, the dynamics of LEC fate commitment remain unclear, and the molecular control of this process remains to be fully understood.

Here, we took advantage of an optimized transgenic line that reports *prox1a* expression and staged analysis of Prox1 protein distribution. Live imaging of precursors in the PCV revealed a cell division preceding secondary sprouting that generates two daughter cells with distinct identities. One daughter remains a VEC in the PCV and the other becomes a LEC and migrates out of the CV, progressively upregulating *prox1a*. These bipotential precursors arise between 30 and 34 hpf, when Prox1

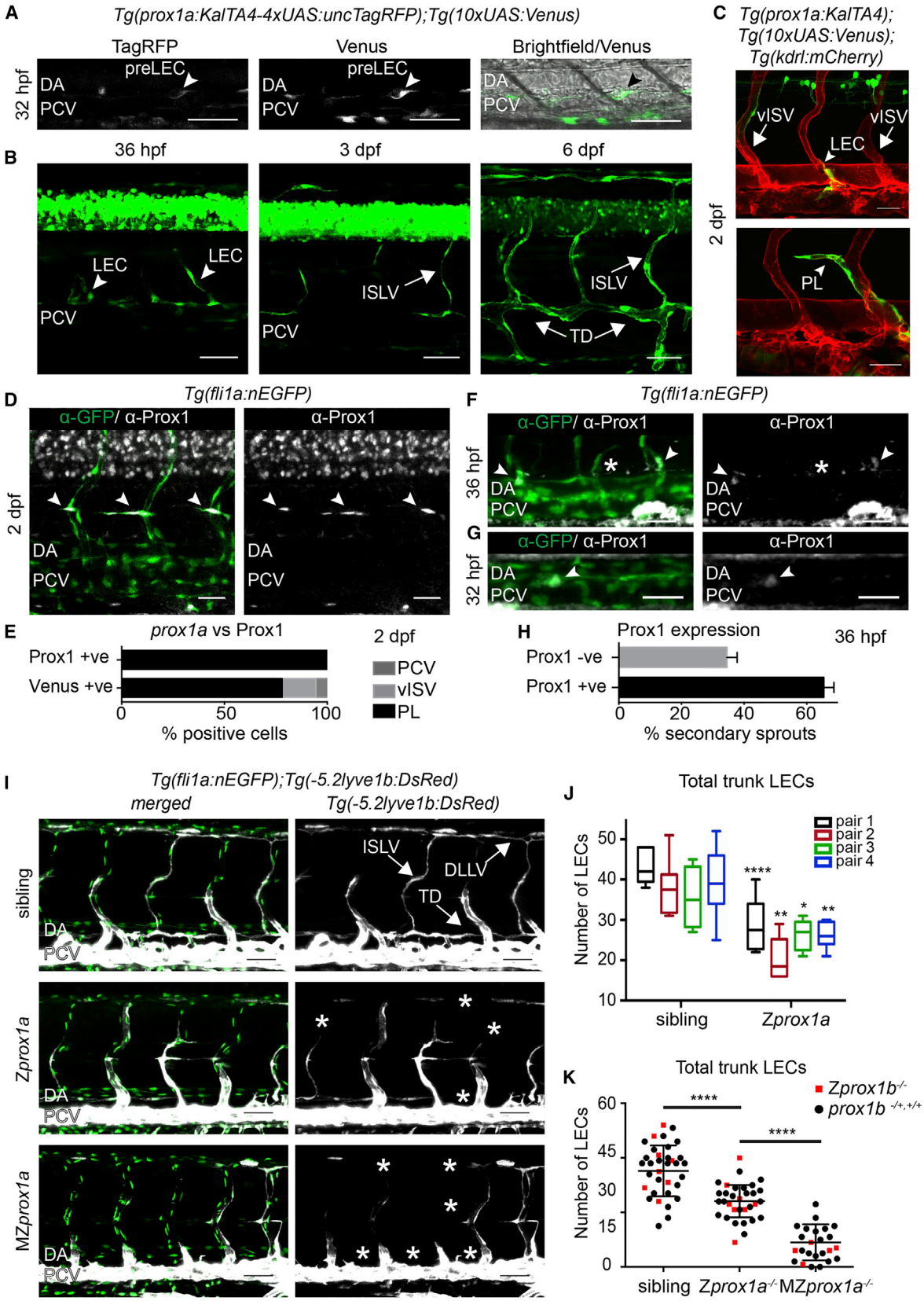

(legend on next page)

expression is initiated. Mechanistically, Vegfc is necessary for precursor cell division and *prox1a*/Prox1 expression, identifying an earlier role for Vegfc than previously reported. The post-division restriction of LEC fate to a single daughter couples cell behavior and signaling dynamics with the restriction of identity in this vascular lineage.

RESULTS

Lymphatic Precursors Express Prox1 Prior to and Concomitant with Sprouting from the PCV

Zebrafish have two Prox1 paralogs, with *prox1a* faithfully marking lymphatics but *prox1b* absent from lymphatics (Dunworth et al., 2014; Tao et al., 2011). It is currently unclear when *prox1a* expression and LEC identity are acquired (Dunworth et al., 2014; Nicenboim et al., 2015; van Impel et al., 2014). To determine the point at which LECs differ from other secondary sprouts, we examined the expression of *Tg(prox1a:KalTA4-4xUAS:uncTagRFP)* (henceforth *prox1a:TagRFP*). We detected expression in cells emerging from the PCV at 36 hpf and occasional weak expression in the PCV at 32 hpf (Figure 1A). As this line relies on KalTA4 and 4xUAS, we enhanced expression levels by introducing a *Tg(10xUAS:Venus)* transgene (Figures 1A and 1B). This improved tool (henceforth *prox1a:Venus*) revealed robust Venus-expressing cells in the wall of the PCV from 32 hpf (Figure 1A). We also generated a transgenic line that did not express TagRFP: *Tg(prox1a:KalTA4);Tg(10xUAS:Venus)* to examine *prox1a*-positive cells present in the dorsal aorta (DA), ISVs, PCV, and secondary sprouts (vISVs and parachordal lymphangioblasts [PLs]) by colocalization with *Tg(kdrl:mCherry)* in the blood vasculature (Figure 1C). At 48 hpf, 78% of *prox1a* expressing cells were PLs (Figures 1C and 1E) 16% were vISVs and 6% were ECs present in the PCV (Figure 1E).

To determine the degree to which this transgene expression reflected endogenous Prox1 distribution, we used immunofluorescence (IF). At 48 hpf, Prox1 protein was found only in PLs at the HM and not in any other trunk vasculature (Figures 1D and 1E), and hence the transgene overrepresents the breadth of Prox1 expression. Comparison of transgene and Prox1-protein-expressing PLs revealed that the transgene is also more mosaic than endogenous Prox1, which is highly restricted and present in all PLs by 2 dpf (Figure 1D; data not shown). These differences are probably due to a combination of the KalTA4-UAS nature of the transgene and the perdurance of Venus reporter protein.

To determine the earliest point when Prox1 protein distribution is restricted, we analyzed 36 hpf embryos when secondary sprouts are emerging from the PCV. We used IF and found that the average percentage of Prox1-positive secondary sprouts per embryo was 65%. The remaining 35% were negative (from n = 15 embryos scored with high resolution across n = 6 segments), indicating that two discrete cell types emerge from the PCV (Figures 1F and 1H). Finally, we found that vascular Prox1 was detectable by 32 hpf (Figure 1G). Hence, ECs express Prox1 preceding secondary angiogenesis, but secondary sprouts are heterogeneous as they emerge from the PCV.

The Critical Role of Prox1 in Lymphangiogenesis Is Conserved in Zebrafish

Prox1 expression serves as a suitable marker of LEC identity in zebrafish, as it does in the mouse. However, the functional contribution of Prox1 homologs in zebrafish has also been contentious (Tao et al., 2011; van Impel et al., 2014). We analyzed the phenotype of *prox1a*^{i278} mutants by precise quantification of total trunk LEC numbers using the overlay of a vascular nuclear EGFP marker and the venous and lymphatic transgenic marker *Tg(−5.2lyve1:DsRed).* As has been previously reported, we observed a mild loss of LECs in *prox1a*^{i278} mutants, with an average reduction of 33% across multiple breeding pairs and up to 41% of LECs at 4 dpf in some pairs (Figures 1I and 1J). This variable phenotype in zygotic mutants is significant, yet

Figure 1. Prox1 Is Expressed and Required in Lymphatic Precursors during Secondary Sprouting

(A) Single confocal projection of a TagRFP-low (left), Venus-high (middle) cell located in the wall of the PCV (bright field, right) at 32 hpf. DA, dorsal aorta; PCV, posterior cardinal vein; pre-LEC, LEC precursor (arrowheads). Scale bars, 50 μm.

(B) Developmental time series of *prox1a:Venus* expression. PCV, posterior cardinal vein; LEC, lymphatic endothelial cell; ISLV, intersegmental lymphatic vessel; TD, thoracic duct. Scale bars, 50 μm.

(C) *Tg(prox1a:KALTA4);Tg(10xUAS:Venus)* expression (green) in a sprouting LEC (above, arrowhead) and a parachordal lymphangioblast (PL, below, arrowhead) at 2 dpf. vISV, venous intersegmental vessel. Scale bars, 30 μm. Blood vasculature in red (*Tg(kdrl:mCherry)*).

(D) Endogenous Prox1-positive (gray) PLs (arrowheads) in the trunk co-labeled by *Tg(fli1a:nEGFP)* (α-GFP, green. Scale bar, 30 μm.

(E) Percentage of total *prox1a:Venus*- and Prox1-expressing (endogenous) cells located in the posterior cardinal vein (PCV), venous intersegmental vessels (vISV), or parachordal lymphangioblasts (PL) at 2 dpf.

(F) Endogenous Prox1-positive (gray) secondary sprouts (arrowheads) and negative secondary sprouts (asterisk) at 36 hpf (*Tg(fli1a:nEGFP)* labeled by α-GFP, green. Scale bar, 30 μm.

(G) Prox1-positive (gray) nuclei located in the dorsal wall of the PCV at 32 hpf (*Tg(fli1a:nEGFP)* labeled by α-GFP, green. Scale bar, 30 μm.

(H) Mean percentage of Prox1-positive and Prox1-negative secondary sprouts per embryo at 36 hpf (Prox1 positive 65.45% ± 3.236 SEM, Prox1 negative 34.55% ± 3.236, n = 15 embryos scored across n = 6 body segments).

(I) Maximum intensity projections of *Tg(fli1a:nEGFP)* (endothelial nuclei, green) and *Tg(−5.2lyve1b:DsRed)* (PCV and lymphatic vessels, gray) in the trunk of sibling (top), Z*prox1a* (middle), and MZ*prox1a* (bottom) mutant embryos at 4 dpf. ISLV, intersegmental lymphatic vessel; TD, thoracic duct; DLLV, dorsal longitudinal lymphatic vessel. Asterisks indicate missing lymphatic structures. Scale bar, 50 μm.

(J) Box and whiskers (min to max) plot of the number of trunk lymphatic nuclei at 4 dpf in sibling and Z*prox1a* mutants (scored across n = 7 body segments): pair1 (n = 6 mutants, n = 10 siblings, 33% reduction), pair2 (n = 7 mutants, n = 6 siblings, 41% reduction), pair3 (n = 6 mutants, n = 4 siblings, 26% reduction), pair4 (n = 9 mutants, n = 7 siblings, 32% reduction).

(K) Total number of trunk lymphatic nuclei at 4 dpf in sibling (n = 34), Z*prox1a* mutants (n = 32) and MZ*prox1a* mutants (n = 24) (mean ± SEM, scored across n = 7 body segments) (t test sibling versus Z*prox1a* ****p < 0.0001 and Z*prox1a* versus MZ*prox1a* ****p < 0.0001) (Z*prox1b* mutants [red], *prox1b* siblings [black]).

much milder than observed in mice (Wigle et al., 2002; Wigle and Oliver, 1999). We hypothesized that the reduced penetrance may be due to *prox1a* maternal deposition, as has been reported (Pistocchi et al., 2008a, 2008b). Hence, we generated maternal zygotic (MZ) *prox1a* mutants by germline transfer (Ciruna et al., 2002). Specifically, we generated germline MZ*prox1a*$^{i278-/-}$;*prox1b*$^{sa0035+/-}$ females and crossed them to *prox1a*$^{i278+/-}$;*prox1b*$^{sa0035+/-}$ males. We observed a vast reduction in the total number of embryonic LECs in MZ*prox1a*^{i278} mutants compared to zygotic (Z) *prox1a*^{i278} mutants and siblings (Figures 1I and 1K). We saw little evidence for a contribution of a zygotic *prox1b* mutant allele to MZ*prox1a* phenotypic severity (red data points in Figure 1K are MZ*prox1a*/Z*prox1b* mutants). Overall, this mutant analysis reveals a robust contribution of Prox1 homologs in zebrafish lymphangiogenesis, confirming the essential nature of the restricted Prox1 expression described above.

The PCV Becomes Structurally Polarized before Prox1 Induction and Secondary Angiogenesis

To better understand the timing of Prox1 induction, we next performed a carefully staged analysis of PCV morphogenesis and Prox1/*prox1a* expression initiation. We examined the distribution of endothelial nuclei in the PCV in double-transgenic *Tg(fli1a:nEGFP);Tg(kdrl:mCherry)* double-transgenic embryos at 26, 30, and 36 hpf (Figures 2A and 2B). Nuclei were evenly distributed around the 26 hpf PCV, but at 30 hpf, and even more prominently at 36 hpf, EC nuclei were increased in number in the dorsal half of the PCV (Figure 2B). Hence, venous morphogenesis involves the establishment of a dorsoventrally polarized tube preceding the dorsal sprouting that occurs during secondary angiogenesis.

We examined Prox1 protein expression at 24, 30, 32, and 36 hpf. Nuclear Prox1 protein was rarely observed at 24 hpf, found in only 3 ventral PCV cells from n = 15 embryos scored across 7 somites (Figures 2C and 2D). At 30 hpf, only 2 dorsal PCV cells were observed from n = 10 embryos, but at 32 hpf, high numbers of Prox1-positive cells were observed in the PCV and highly enriched in the dorsal PCV. Further increased numbers of dorsal Prox1-positive cells were observed by 36 hpf (Figures 2C and 2D). We also quantified Prox1 fluorescence intensity at these time points relative to expression in nearby trunk neurons (Figure S1). We found that Prox1 expression progressively increases in developing LEC precursors (Figures 2E and 2F). These data demonstrate a predominantly dorsal induction of Prox1 protein expression in the PCV, following polarization of the vein, between 32 and 36 hpf (Figure 2G).

Interestingly, when we examined the *prox1a:Venus;Tg(kdrl:mCherry)* line, we found that transgene expression was broader throughout the PCV than endogenous protein distribution from 24 to 30 hpf (Figure S1). By 36 hpf, the transgene was more highly enriched in dorsally sprouting cells (Figure S1), again suggesting that the transgene overrepresents distribution of Prox1 protein at early, but not later, stages. Importantly, both endogenous Prox1-expressing cells in the PCV and transgene-expressing cells were endothelial by co-expression of *Tg(fli1a:nEGFP)*, *Tg(−5.2lyve1:DsRed)* and *Tg(kdrl:mCherry)* (Figures 1C, 2A, and S1).

Prox1a-Positive Precursors Divide in the PCV and Give Rise to Both Lymphatic and Venous Daughter Cells

The dynamic process of commitment to LEC identity by VECs has not previously been observed in real time during development. We performed live imaging of *prox1a:Venus* beginning at 30 hpf. Analysis of time-lapse movies revealed a distinctive division of *prox1a*-positive cells in the PCV prior to sprouting. Following this, daughter cells behaved asymmetrically, as one daughter remained in the vein while the other migrated dorsally to the HM (Movie S1). Quantification of cell behavior during PL formation from n = 19 independent movies revealed that this daughter cell behavior followed a cell division in 84% of cases in *prox1a*-expressing cells (Figure 3B). In the remaining 16% of cases, a cell division preceded both daughter cells migrating to the HM, and we did not observe PL formation without a preceding cell division in PCV (Figure 3B).

To determine if these distinct daughter cell behaviors reflect different molecular identities following cell division, we quantified *prox1a* reporter expression. We injected DNA encoding nuclear H2AmCherry and membranous EGFP driven from a 10xUAS element into *prox1a:TagRFP* (uncTagRFP is nuclear excluded, KalTA4 is present) and labeled individual *prox1a*-positive nuclei over time (Figure 3A; Movie S2). We quantified average nuclear pixel intensity of H2AmCherry in ECs throughout the time lapse and found that after cell division, the nucleus of the dorsal migrating daughter cell displayed increasing *prox1a* compared with the ventral daughter (Figures 3A′ and 3C; Movie S3). Demonstrating reproducibility, the ratio of average *prox1a* pixel intensity per nucleus for ‘‘dorsally migrating daughter cell (LEC)’’ over ’’ventral daughter cell (VEC)’’ continuously increased after division across multiple movies (Figure 3D). There were no consistent changes in nuclei Z-position or ellipticity during these movies (Figures 3E, 3F, and S2). The loss of expression in the venous daughter was consistent with a lack of *prox1a*/Prox1 in the PCV by 48 hpf (see Figures 1C–1E). In addition, we analyzed endogenous Prox1 levels in isolated, closely neighboring *prox1a:Venus*-positive cells (doublets) located in the PCV at 36 hpf. We found that in 76% of doublets, Prox1 protein was restricted to the putatively sprouting, dorsal *prox1a:Venus*-positive LEC and not present in the *prox1a:Venus*-positive VECs in the PCV wall, suggesting rapid restriction of Prox1 expression to one daughter cell post-division (Figures 3G and 3H).

Together, these data show that bipotential *prox1a:Venus*/Prox1-positive cells divide in the PCV from 30 hpf, giving rise to daughter cells with asymmetric behaviors and identities. One daughter is a VEC and remains in the PCV and the other is a LEC and migrates dorsally, elevating *prox1a* transcription and Prox1 protein levels.

Live Imaging of PCV Nuclei Confirms Bipotential Precursor and Daughter Cell Dynamics

We next tracked individual nuclei using the *Tg(fli1a:GALFF);Tg(4xUAS:RFP);Tg(fli1a:nEGFP)* line (Figure 4A and 4A′; Movie S4). We examined n = 11 movies and were able to accurately track both LECs and VECs after division in just n = 3 due to the high concentration of dorsal nuclei in the PCV. These movies confirmed behaviors seen using *prox1a:Venus*, with division preceding dorsal migration of one daughter and the other daughter

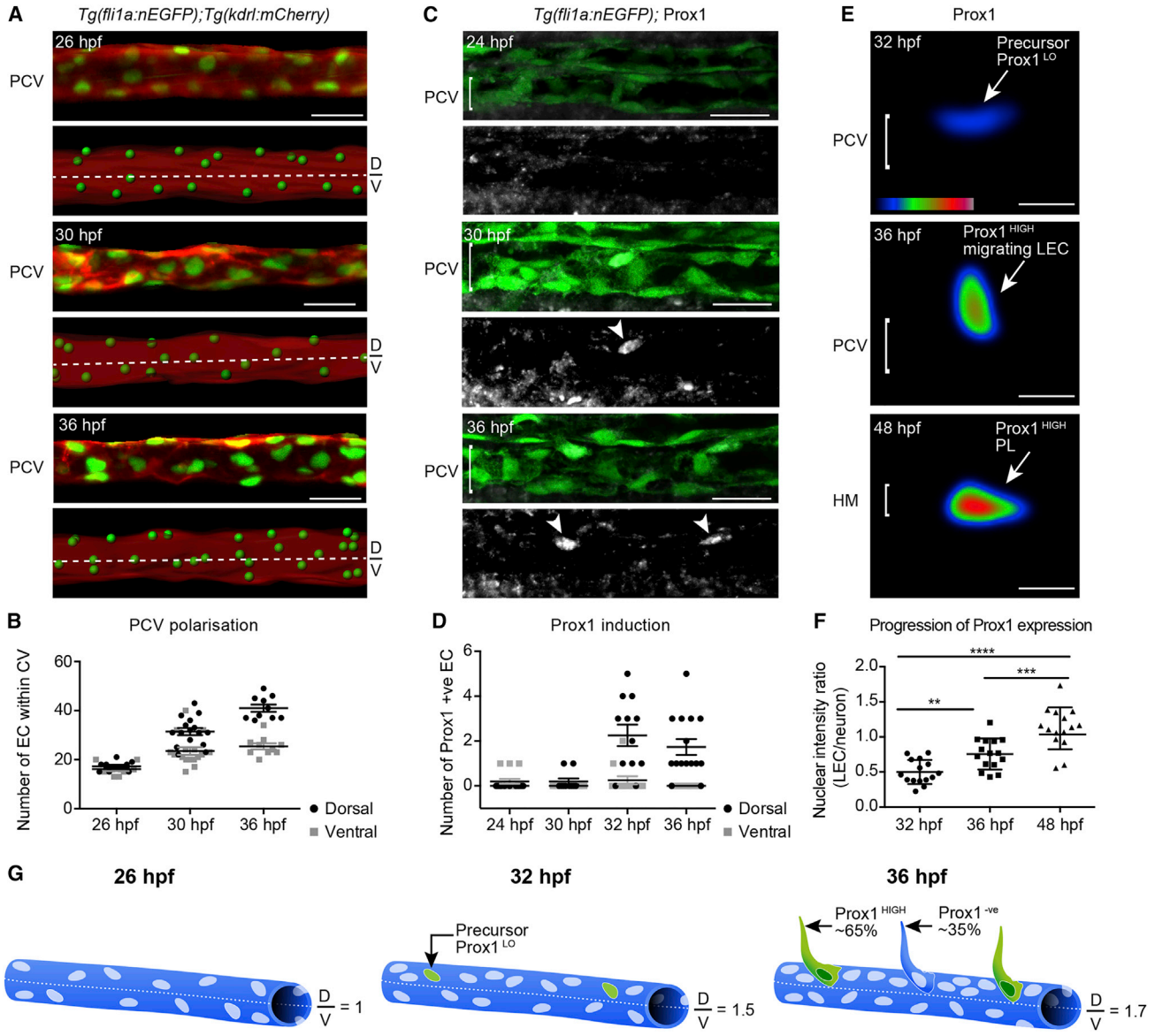

Figure 2. The PCV Becomes Structurally Polarized and Initiates Prox1 Expression before Secondary Angiogenesis

(A) Confocal projection of *Tg(fli1a:nEGFP);Tg(kdrl:mCherry)* labeling endothelial cell (EC) nuclei (green) and membrane (red) showing the PCV (upper) and rendered signal (lower) at 26, 30, and 36 hpf (scored across 3 body segments). D, dorsal; V, ventral. Scale bar, 30 μm.

(B) Quantification of EC number in the dorsal (black circles) and ventral (gray squares) halves of the PCV scored in lateral projections at 26 hpf (n = 10), 30 hpf (n = 16), and 36 hpf (n = 10) (scored across 3 body segments) (mean ± SEM).

(C) Endogenous Prox1 (gray, lower) in the trunk vasculature of *Tg(fli1a:nEGFP)* embryos (α-GFP, green, top) at 24, 30, and 36 hpf (scored across 3 body segments). Scale bar, 30 μm.

(D) Quantification of the number of Prox1 positive ECs in dorsal and ventral halves of the PCV at 24 hpf (n = 15), 30 hpf (n = 10), 32 hpf (n = 12), and 36 hpf (n = 12) (scored across 3 body segments) (mean ± SEM).

(E) Heatmap of average intensity projection of Prox1-positive ECs at 32, 36, and 48 hpf. Scale bar, 10 μm.

(F) Quantification of Prox1 protein expression intensity in *Tg(fli1a:nEGFP)*-positive ECs relative to Prox1 neuronal expression at stages indicated (t test: 32 hpf versus 36 hpf **p = 0.0013, 36 hpf versus 48 hpf ***p = 0.0007, and 32 hpf versus 48 hpf ****p < 0.0001; mean [SD]).

(G) Schematic representation of PCV polarization and Prox1 induction.

remaining in the PCV (Figures 4A and 4A′). To improve this analysis, we generated cellular mosaic embryos by transplantation (Figure 4B). We time-lapse imaged mosaic embryos and tracked EC nuclei through to dorsal migration to the HM, when they can be identified as PLs based on location (Figure 1C; Movies S4 and S5). This approach revealed asymmetric behavior of daughter cells post-precursor division in 83% of cases from n = 12 divisions (Figures 4C and 4D; Movies S4 and S5); additionally, the

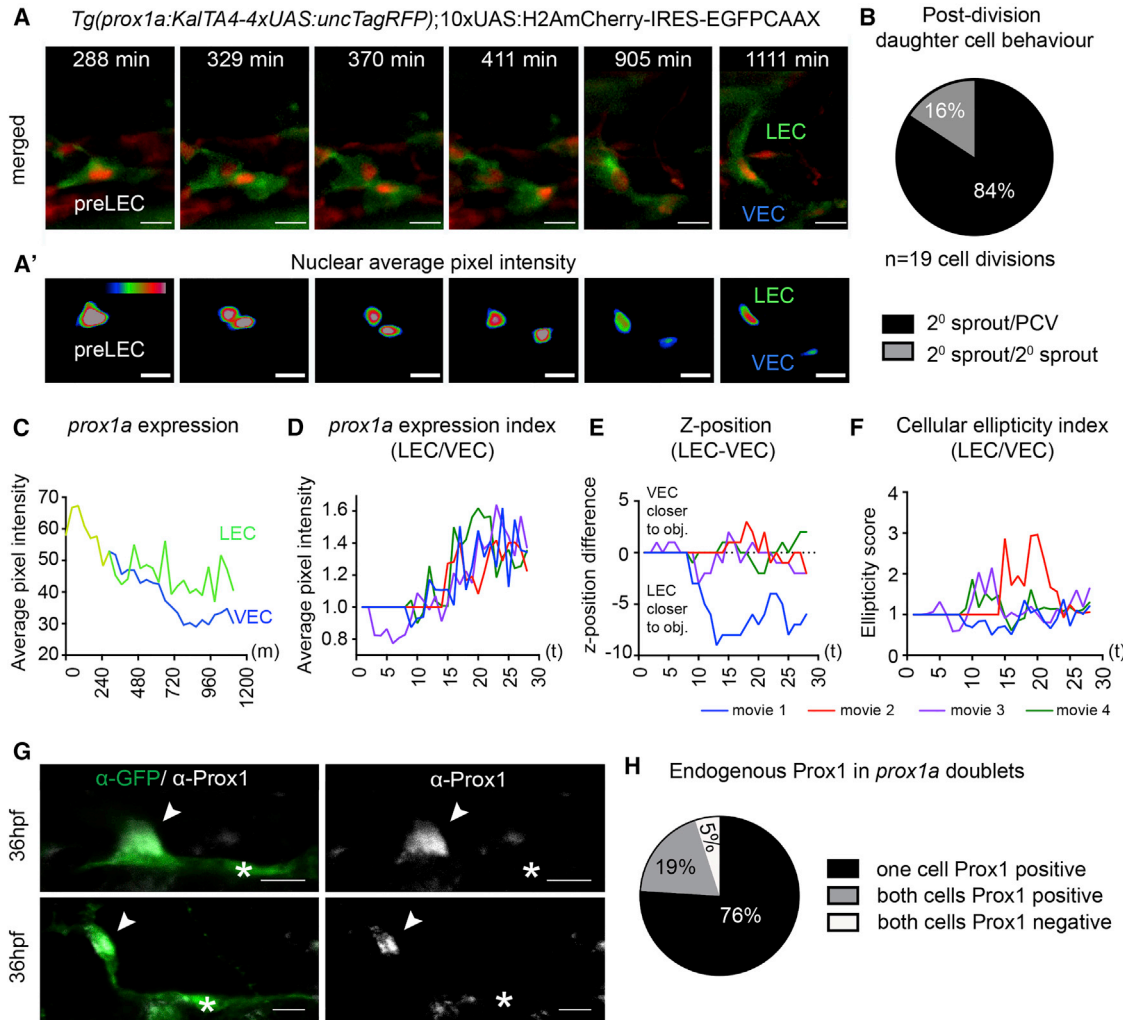

Figure 3. Bipotential *prox1a*-Positive Precursors in the PCV Give Rise to LECs and VECs

(A) Maximum intensity projections from time lapse of cell division in a *prox1a*-positive pre-LEC *Tg(prox1a:TagRFP)* labeled with 10xUAS:H2AmCherry-IRES-GFPCAAX. Nuclei are red and membranes are green. Scale bars, 15 μm.

(A′) Heatmap of average fluorescent intensity of *prox1a:H2AmCherry* nuclei depicted in (A) (scale bars, 15 μm).

(B) Percentage daughter cell behaviors observed post-/pre-LEC division (84%, one cell migrating dorsally [2° sprout] and one remaining in the PCV; 16%, both daughter cells migrate dorsally; and 0%, both daughter cells remaining the PCV [n = 19 cell divisions]).

(C) Average nuclear *prox1a:H2AmCherry* fluorescent intensity per pixel over time for movies shown in (A) and (A′), prior to division (yellow), LEC (green), and VEC (blue).

(D) Index of LEC/VEC *prox1a:H2AmCherry* average nuclear fluorescent intensity per pixel over time taken from n = 4 independent time-lapse movies. Each color represents an independent division event (movie 1, blue; movie 2, red; movie 3, purple; and movie 4, green).

(E) Difference in z-position of the LEC versus the VEC nucleus over time in corresponding time-lapse movies shown in (D).

(F) Index of LEC/VEC nuclear ellipticity (longest axis/shortest axis) over time of corresponding time-lapse movies in (D).

(G) Endogenous Prox1 (gray) in *prox1a:Venus* doublets (two cells side by side in isolation in the PCV [green]) at 36 hpf (a Prox1-positive cell [arrowhead]/Prox1-negative cell [asterisk], n = 18; upper and lower are two different examples. Scale bars, 15 μm.

(H) Percentage of different Prox1 protein distribution patterns in *prox1a* positive doublets at 36 hpf (n = 21 doublets scored).

majority of divisions occurred in the dorsal half of the PCV (Figure 4E). Importantly, these movies spanned the period when Prox1 expression turns on in the PCV, through to stages when Prox1 expression becomes absent from the PCV (from 28 hpf up to 3 dpf), and we did not observe additional divisions of VEC daughter cells to contribute additional LECs.

Using this approach, we also observed nuclear dynamics of cells that contribute to the venous ISVs. 60% of cells migrating into a developing vISV were derived from a cell division in which one daughter cell remained in the PCV (analogous to LEC precursor behaviors), 10% were derived from a cell division in which both cells contributed to the forming vISV, and 30% of nuclei were not immediately derived from a cell division (n = 10 movies; Figures 4F and S2; Movie S6), a scenario not seen in LEC precursor behaviors. Finally, we quantified nuclear expression intensity in these *Tg(fli1a:nEGFP)* ECs (Figures 4G–4I; Movie S7). We saw

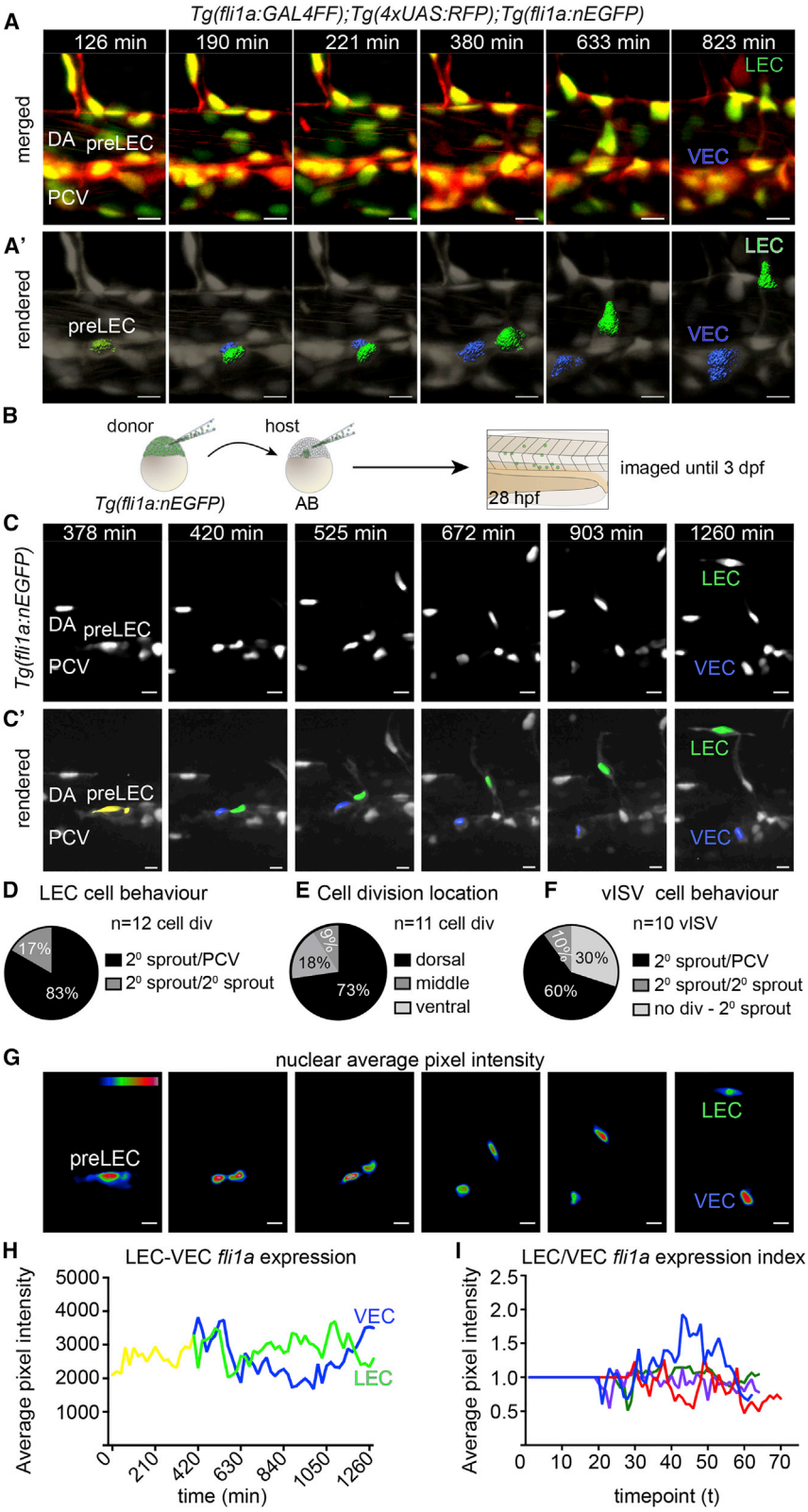

Figure 4. Endothelial Nuclear Dynamics Reveal Bipotential Precursor Behaviors

(A) Maximum intensity projections from a time lapse of a dividing LEC precursor (pre-LEC) in the dorsal wall of the posterior cardinal vein (PCV), with *Tg(fli1a:GALFF);Tg(4xUAS:RFP)* in red and *Tg(fli1a:nEGFP)* in green (scale bars, 10 μm). DA, dorsa aorta; VEC, venous endothelial cell.

(A′) Rendered *Tg(fli1a:nEGFP)* nuclei (gray) corresponding to A (pre-LEC, yellow; VEC, blue; LEC, green. Scale bars, 10 μm.

(B) Schematic representation of transplantation approach with genotypes and stages indicated.

(C) Maximum intensity projections from a time lapse of mosaically *Tg(fli1a:nEGFP)*-labeled embryo showing a dividing pre-LEC in the PCV. Scale bars, 12 μm.

(C′) Rendered *Tg(fli1a:nEGFP)* nuclei (gray) corresponding to (C) (pre-LEC, yellow; VEC, blue; LEC, green). Scale bars, 10 μm.

(D) Percentage of daughter cell behaviors post pre-LEC division (83%, one daughter cell migrating dorsally [2° sprout] and one remaining in the PCV; 17%, both migrate dorsally; and 0%, both remaining in the PCV, from n = 12 cell divisions).

(E) Location of pre-LEC cell divisions within the PCV from (D). 73% of divisions occur in the dorsal half of the PCV, 18% at the midline (as shown in Figure 2), and 9% in the ventral half (n = 11 cell divisions).

(F) Behavior for ECs contributing to vISVs. 60% of dorsal migration is preceded by cell division with one daughter cell migrating dorsally (2° sprout) and one remaining in the PCV, 10% is migration with both daughter cells migrating dorsally, and 30% is not preceded by cell division (from n = 10 movies).

(G) Heatmap of average fluorescence intensity of *Tg(fli1a:nEGFP)* nuclei depicted in (C) and (C′). Scale bars, 12 μm.

(H) Average nuclear *Tg(fli1a:nEGFP)* fluorescent intensity per pixel over time for movies shown in (C) and (C′).

(I) Index of LEC/VEC *Tg(fli1a:nEGFP)* average nuclear fluorescence intensity per pixel over time taken from n = 4 time-lapse movies from mosaic nuclei. Each color represents an independent cell division.

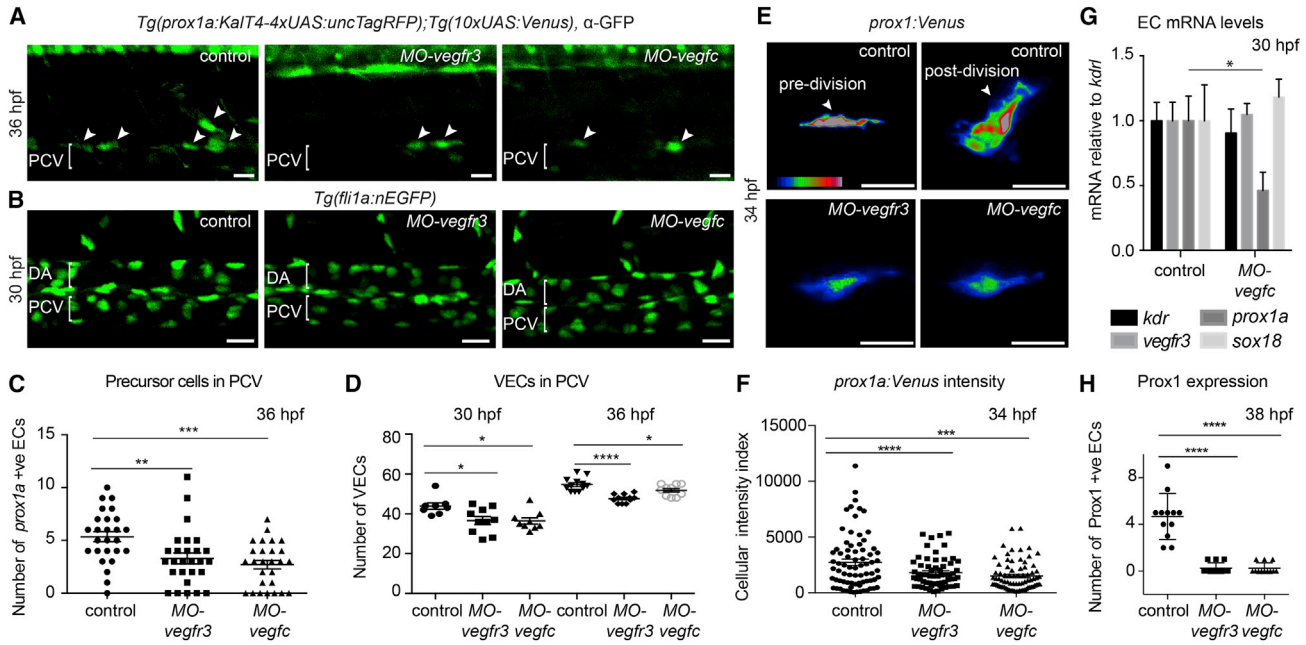

Figure 5. Vegfc Signaling Is Necessary for VEC Proliferation and Prox1 Expression

(A) Maximum intensity projection of *prox1a:Venus* (α-GFP, green) at 36 hpf in control, *MO-vegfr3*, and *MO-vegfc* embryos in LEC precursors (arrowheads). PCV, posterior cardinal vein.

(B) Maximum intensity projection of *Tg(fli1a:nEGFP)* at 30 hpf in control, *MO-vegfr3*, and *MO-vegfc* embryos across two somites in the posterior cardinal vein (PCV). DA, dorsal aorta.

(C) Quantification of the number of *prox1a* positive LEC precursors (mean ± SEM) in *MO-vegfr3*- (n = 27) and *MO-vegfc*-injected (n = 27) embryos compared to controls (n = 26). Asterisks indicate significance (ANOVA *p = 0.0456, ****p < 0.0001).

(D) Quantification of VEC number at 30 and 36 hpf in *Tg(fli1a:nEGFP)* in control (n = 8, n = 12), *MO-vegfr3* (n = 10, n = 11) and *MO-vegfc* (n = 9, n = 10; mean ± SEM). Asterisks indicate significance (ANOVA *p = 0.0165, ****p = 0.0168).

(E) Fluorescence intensity of *prox1a:Venus* in confocal projections of lymphatic precursors in *MO-vegfr3* and *MO-vegfc* embryos compared with control cells pre- and post-division.

(F) Quantification of *prox1a:Venus* average intensity per pixel in individual *MO-vegfr3* (n = 62), *MO-vegfc* (n = 76), and control precursor cells (n = 75; mean ± SEM). Asterisks indicate significance (ANOVA **p = 0.0058, ****p < 0.0001).

(G) mRNA expression of *kdr*, *vegfr3*, *prox1a*, and *sox18* in FACS EC populations from control and *MO-vegfc* embryos at 30 hpf. Graph represents gene expression relative to *kdrl* from three biological repeats (mean ± SEM).

(H) Number of Prox1-protein-positive EC nuclei at 38 hpf in *MO-vegfr3* (n = 12), *MO-vegfc* (n = 12), and control precursor cells (n = 12; mean ± SEM) scored across six somites. Asterisks indicate significance (ANOVA ****p < 0.0001).

no consistent changes in expression between LEC and VEC daughter cells (Figures 4G–4I), confirming the specificity of the *prox1a* findings above.

Vegfc Drives Bipotential Precursor Cell Division and Is Necessary for Prox1 Expression

Given that restriction of LEC identity occurs with or immediately following precursor division, we investigated if Vegfc is important for promoting this division. Vegfc is essential during LEC sprouting from the PCV (Hägerling et al., 2013; Hogan et al., 2009a; Karkkainen et al., 2004) and regulates VEC proliferation (Helker et al., 2013; Koltowska et al., 2015). To determine if loss of Vegfc-Vegfr3 signaling influences LEC specification, we injected *prox1a:Venus* embryos with the morpholino oligomers *MO-vegfr3* and *MO-vegfc*, which efficiently phenocopy known mutants (Kok et al., 2015; Le Guen et al., 2014). We found that *prox1a:Venus*-positive cells were still present in the PCV but significantly reduced in number (Figures 5A and 5C). We quantified VEC numbers in the PCV and observed at 30 hpf a general reduction of VEC numbers in these morphants that was further pronounced at 36 hpf (Figures 5B and 5D). These data suggest that Vegfc establishes LEC precursor numbers by generally promoting VEC proliferation.

Although some *prox1a* transgene transcription was initiated in Vegfc morphants, we quantified the intensity of *prox1a:Venus* expression in LEC precursors in *MO-vegfc*- and *MO-vegfr3*-injected embryos. We observed a dramatic reduction in expression intensity compared with control *prox1a:Venus*-positive precursor cells at 34 hpf (Figures 5E and 5F). Importantly, *prox1a:Venus* intensity was reduced in non-dividing morphant cells compared to both dividing and yet undivided control precursors (Figure 5E). *prox1a:Venus* expression in neurons was unchanged (Figure S3). We also performed qRT-PCR on fluorescence activated cell-sorted (FACS) ECs from control and *MO-vegfc* embryos and found a decrease in *prox1a* RNA levels (Figure 5G). Strikingly, when we analyzed Prox1 protein distribution during stages of initiation, we found an absence of EC nuclear Prox1 in *MO-vegfc*- and *MO-vegfr3*-injected embryos (Figures

5H and S3). Together, these findings indicate that Vegfc signaling controls *prox1a*/Prox1 expression in the PCV, exerting control during the earliest stages in LEC commitment.

Vegfc Is Sufficient to Induce Prox1 Expression in Embryonic VECs

To understand whether Vegfc signaling is sufficient to modulate Prox1 expression, we crossed *prox1a:TagRFP* to the *Tg(10xUAS:vegfc)* strain (henceforth *vegfc-induced*). *prox1a* is expressed broadly in somites, neurons, endodermal organs, and ECs in the trunk; hence, KalTA4 will induce Vegfc expression broadly, in all tissues where *prox1a* is expressed. We observed the previously reported Vegfc-driven venous hyper-sprouting (Le Guen et al., 2014) and quantified EC nuclei and *prox1a*-expressing cells. At 4 dpf, we observed increased VEC numbers and, remarkably, we observed ectopic expression of *prox1a* throughout venous, but not arterial, endothelium (Figures 6A and S4). Supporting the specificity of this phenotype, we observed ectopic Prox1 protein (data not shown), and depletion of Vegfr3 or Ccbe1 rescued the phenotype (Jeltsch et al., 2014; Le Guen et al., 2014) (Figure S4; Table S1). Using chemical inhibitors, we found that the phenotype required intact Mek/Erk signaling, but not Notch signaling or the presence of Sox18 and Sox7 (Figure S4; Table S1). These data demonstrate that Vegfc is sufficient to induce *prox1a* expression in zebrafish VECs. In this overexpression context, Vegfc signals through Vegfr3-Mek-Erk to induce VEC proliferation and *prox1a*.

Vegfc Signaling Regulates Prox1 Expression and Daughter Cell Behavior

Having observed that Vegfc is sufficient to induce *prox1a* expression in embryonic VECs by 4 dpf, we investigated earlier stages. We first quantified EC nuclei in the PCV of *vegfc-induced* embryos at 30 and 36 hpf. Although at 36 hpf the number of PCV ECs had doubled in *vegfc-induced* embryos, in 30-hpf embryos, there was no change in cell number (Figure 6B). Despite this, ectopic expression of *prox1a:Venus* and Prox1 protein could be detected throughout the PCV at both 30 and 36 hpf (Figures 6C–6E). Furthermore, at the level of the PCV, *prox1a:Venus* doublets were consistently both positive for Prox1 in *vegfc-induced* embryos (Figure 6E′), unlike sibling controls (Figures 3G and 3H).

We performed time-lapse imaging of the PCV in *prox1a:Venus;vegfc-induced* embryos (Figure 6F; Movies S8 and S9). Wild-type daughter cells presented typical asymmetric behaviors post division (Figure 6F, top, and Figures 3 and 4; Movies S1, S2, S3, S4, S5, S7, and S8). However, in *vegfc-induced* embryos we saw a dramatic induction of VEC proliferation and *prox1a* expression. In this context, when we examined individual, isolated precursor cell divisions, this asymmetric behavior was only observed following 42% of divisions compared with 84% in genetic background-matched controls (Figures 6G and 3B). 35% of divisions gave rise to two dorsally migrating daughters and in 23% of cases the two daughters remained in the PCV in *vegfc-induced* embryos (Figure 6F, bottom, and Figure 6G; Movies S8 and S9). These data suggest that Vegfc levels determine *prox1a*/Prox1 expression levels at stages during the restriction of LEC identity and also influence cell behavior at these stages.

DISCUSSION

Establishing LEC Identity in Zebrafish

Here, we applied live imaging techniques to reveal an undescribed cellular mechanism during zebrafish lymphangiogenesis. Prox1-positive cells form a bipotential precursor pool in the vein and precursors undergo a Vegfc-regulated cell division to give rise to both LECs and VECs (see model summarized in Figure 7). This cell behavior ensures the maintenance of PCV cell number, allowing for the remarkable exodus of LECs from the dorsal wall of the PCV to generate a new vascular lineage.

Importantly, this alters our understanding of how commitment to LEC fate occurs. Specification is defined as a labile phase in which a cell becomes capable of differentiating autonomously in a neutral environment and is a key step in cellular commitment preceding determination (Gilbert, 2000). Prox1-positive cells in the zebrafish PCV are capable of giving rise to two different cell types: LECs and VECs. Hence, these cells are competent but not specified to a single lineage. They are bipotential when present in the PCV, despite their expression of Prox1. Following division, specified LECs begin dorsal migration from the PCV, and these cells upregulate Prox1, further committing as LECs. Nevertheless, 65% of cells leaving the vein during secondary angiogenesis express Prox1 (Figure 1H) but only 50% will form LECs (Bussmann et al., 2010). This suggests plasticity in commitment during secondary sprouting. It will be interesting to understand if the progressive commitment to LEC identity involves additional, hard-wired, molecular cues or is stochastic in nature.

Interestingly, the PCV becomes structurally polarized preceding secondary angiogenesis. These data imply either a patterned dorsal proliferation of ECs in the PCV or a net movement of cells from the ventral to dorsal half of the PCV between 26 and 30 hpf. As proliferation of PCV ECs is equally distributed throughout the vessel (Nicenboim et al., 2015), the later seems more likely. The recently described movement of *fli1a*-, *lyve1*-, and *flt1*-positive cells from the ventral to dorsal PCV in the study by Nicenboim et al. occurs from 24 hpf (Nicenboim et al., 2015), well before the divisions reported here. It is likely that these ventral wall angioblast divisions and the movement of daughter cells from the ventral to dorsal PCV contribute to vessel polarization. We here report both induction of Prox1 expression and cell divisions that occur later, following polarization of the PCV and largely occurring in the dorsal PCV. Hence, we suggest that commitment to LEC fate is a dynamic process that follows the early division of ventral angioblasts, providing ECs to the dorsal PCV (from 24 hpf), and involves induction of Prox1 expression in bipotential precursors (from 30 to 32 hpf), precursor cell division (from 32 hpf), and the exodus of LECs from the PCV (from 36 hpf). Overall, the process represents a mechanism by which cellular commitment occurs progressively at sequential locations through the embryo as development proceeds.

Vegfc Signaling as an Upstream Regulator of Prox1

Interestingly, we find that Vegfc signaling acts upstream of Prox1 and is both necessary for normal Prox1 expression and high Vegfc is sufficient to induce Prox1 in developing VECs. However, vISVs do not go on to express Prox1 despite responding to

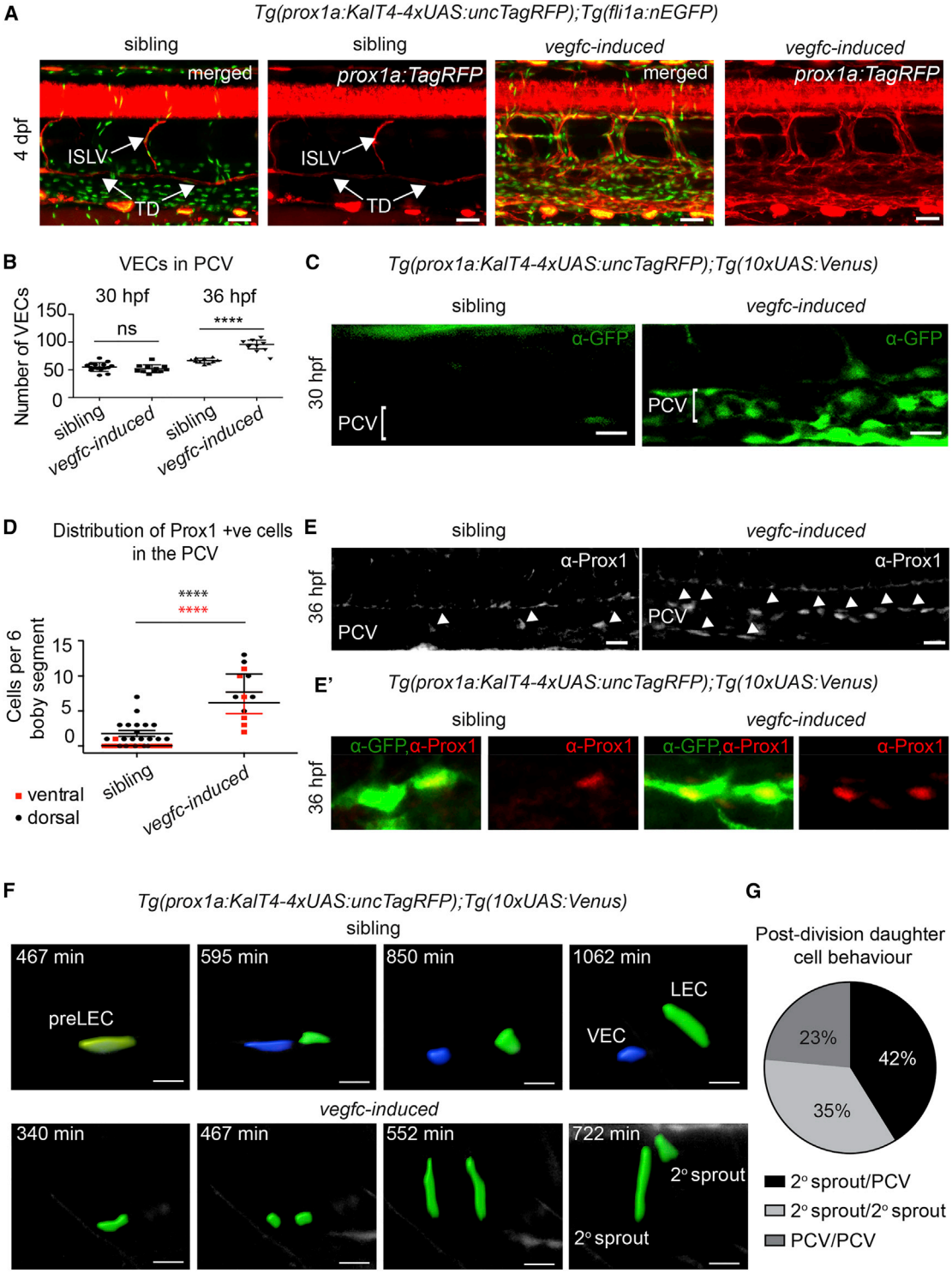

Figure 6. Vegfc Is Sufficient to Induce Prox1 Expression and Regulate Daughter Cell Behaviors

(A) Maximum intensity projections of *Tg(fli1a:nEGFP)* in green and *prox1a:TagRFP* in red, with *Tg(10xUAS:vegfc)* (n = 8, *vegfc-induced*) and sibling (n = 8) embryos at 4 dpf. ISLV, intersegmental lymphatic vessels; TD, thoracic duct. Scale bar, 40 μm.

(B) Quantification of VEC number at 30 and 36 hpf using *Tg(fli1a:nEGFP)* in sibling (30 hpf, n = 16; 36 hpf, n = 10 embryos) and *vegfc-induced* embryos (30 hpf, n = 11; 36 hpf, n = 10 embryos) (ANOVA ****$p < 0.0001$; mean [SD]).

(legend continued on next page)

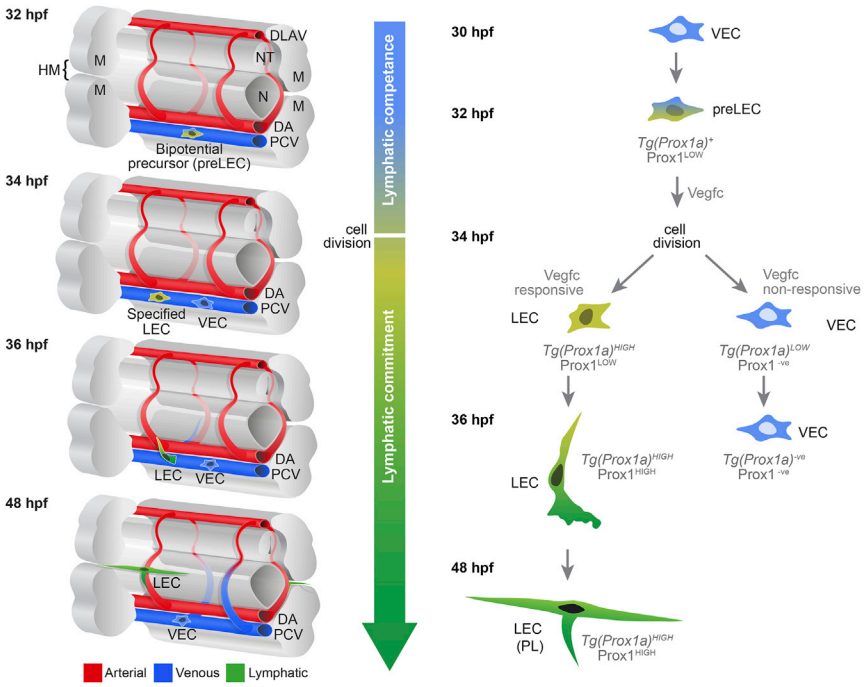

Figure 7. A Model of LEC Commitment in Zebrafish

Representation of tissue contributions during zebrafish lymphatic development (left panel) and of cellular events during LEC commitment (right panel) between 32 and 48 hpf.

From 30 to 32 hpf, cells in the PCV induce Prox1. These bipotential LEC precursors (pre-LECs) give rise to LECs and VECs upon Vegfc-dependent cell division. The VEC will remain in the PCV. The LEC migrates dorsally in response to Vegfc. Progressive upregulation of Prox1 and fate commitment in the emergent LEC occur during migration to the HM. At the HM, LECs have been referred to as parachordal lymphangioblasts (PLs) or parachordal cells (PACs) indicative of their location. LECs/PLs will give rise to the trunk lymphatic network.

Vegfc. It will be important in future studies to determine how vISVs remain as blood vascular endothelium and whether this is a default state in the absence of Prox1 or an actively regulated process.

Most of our current understanding of LEC fate comes from studies in mouse where LECs are thought to be specified within the CV by obtaining PROX1 expression (Srinivasan and Oliver, 2011; Wigle and Oliver, 1999). Once specified, LECs sprout from the CV to give rise to the lymphatics (Hägerling et al., 2013; Karkkainen et al., 2004; Wigle and Oliver, 1999). The induction of PROX1 in mouse is regulated by a distinct mechanism from the maintenance of PROX1 in specified murine LECs (François et al., 2008; Johnson et al., 2008; Srinivasan et al., 2010). Interestingly, early maintenance of PROX1 requires a regulatory feed-forward relationship between VEGFR3 and PROX1 in mice (Srinivasan et al., 2014). This previous finding and our data would be consistent with a mechanism in which zebrafish LEC daughter cells progressively elevate Vegfr3 signaling, consequently elevating Prox1 expression and hence LEC fate is progressively reinforced as these cells sprout from the PCV. However, in knockout mice with reduced VEGFC signaling, Prox1 expression is still initiated (Bos et al., 2011; Hägerling et al., 2013; Karkkainen et al., 2004), but here we see reduced or absent Prox1 induction in zebrafish depleted for Vegfc/Vegfr3 signaling (Figure 5). One difference in zebrafish may be the role played by maternally deposited Prox1. It is possible that the maternal contribution (Figures 1I–1K) is sufficient to initiate zygotic Prox1 in zebrafish, a very different scenario to induction of PROX1 transcription in mice. The precise role of maternal Prox1 and the initial control of Prox1 induction in the zebrafish requires further analysis before a direct comparison can be drawn.

Asymmetric Cell Division or Asymmetric Daughter Cell Behaviors?

The division of bipotential precursors that we report here generates daughter cells that have different behaviors and different identities. However, we have not shown that the cell division itself is asymmetric rather than the asymmetric assignment of identity following division. We do note that in the observed scenario, an initial asymmetry needs to be present in the system. How is asymmetry established? One possibility is the shuttling of a determinant into one daughter cell during the division of bipotential LEC/VEC precursors. Such a scenario occurs with the asymmetric localization of the Prox1 homolog Prospero during *Drosophila* neuroblast division (Hirata et al., 1995; Yu et al.,

(C) Confocal projections of *prox1a:Venus* expression in the posterior cardinal vein (PCV) in sibling (n = 2) and *vegfc-induced* (n = 8) embryos at 30 hpf. Scale bar, 20 μm.

(D) Number of Prox1-positive (antibody staining) cells in dorsal or ventral PCV in sibling (n = 20) and *vegfc-induced* (n = 6) embryos scored across six somites at 36 hpf. *vegfc-induced* embryos showed a 5-fold increase in dorsal wall cells and further increase in ventral wall cells (mean ± SEM).

(E) Confocal projections of endogenous Prox1 expressing cells (gray) in *vegfc-induced* (n = 10) and sibling embryos (n = 18) (scale bar, 20 μm) at 36 hpf.

(E′) Confocal projections of *prox1a:Venus*-expressing cells co-stained with endogenous Prox1. In *vegfc-induced* (n = 11) embryos, Prox1 was present in all *prox1a:Venus*-positive cells compared with control cells (n = 8).

(F) Confocal projections from time lapse of sibling (top) and *vegfc-induced* (bottom) embryos showing rendered *prox1a:Venus* cells (pre-LEC, yellow; VEC, blue; LEC, green. Scale bar, 20 μm.

(G) Quantification of daughter cell behaviors from *prox1a*-positive precursors in *vegfc-induced* embryos visualized in time lapse from 30 hpf. In 42%, one cell migrated dorsally (2° sprout) and one remained in the PCV; in 35%, both daughter cells migrated dorsally; and in 23%, both cells remained in the PCV (from n = 17 cell divisions scored in n = 10 movies).

2006). Another possibility would be through tip-stalk cell-like signaling to select one active, Vegfc-responsive and one inactive, less responsive cell post-division (e.g., reviewed in Geudens and Gerhardt, 2011). While hypotheses such as these are attractive, significantly increased depth of resolution will be needed to directly observe such mechanisms during bipotential precursor division.

EXPERIMENTAL PROCEDURES

Zebrafish Strains and Transgenesis

Animal work followed guidelines of the animal ethics committees at the University of Queensland. Published transgenic lines and mutants were *Tg(kdrl:Hsa.HRAS-mCherry)*^{s916} (Hogan et al., 2009a), *Tg(fli1a:nEGFP)*^{y7} (Lawson and Weinstein, 2002), *Tg(−5.2lyve1b:DsRed)*^{nz101} (Okuda et al., 2012), *Tg(fli1a:GALFF)*^{ubs3} (Sauteur et al., 2014), *prox1a*^{i278}, *prox1b*^{sa0035} (van Impel et al., 2014), and *TgBAC(prox1a:KalTA4-4xUAS-ADV.E1b:TagRFP)*^{nim5} (Dunworth et al., 2014; van Impel et al., 2014). *TgBAC(prox1a:KalTA4-4xUAS-ADV.E1b:TagRFP)*^{nim5}, *Tg(fli1a:GALFF)*^{ubs3}, *Tg(4xUAS:RFP)*, and *prox1a*^{i278}, *prox1b*^{sa0035} were kindly provided by the Ober, Affolter, Bakkers, and Ingham laboratories, respectively. For details on generation of *Tg(prox1a:KalTA4)*^{uq3bh}, *Tg(10xUAS:vegfc)*^{uq2bh}, and MZ*prox1a*^{uq4bh}, see Supplemental Experimental Procedures.

Genotyping and Construct Generation

Tg(10xUAS:vegfc)^{uq2bh}, *prox1a*^{i278} and *prox1b*^{sa0035} genotyping primers are described in Supplemental Experimental Procedures. 10xUAS:vegfc plasmid DNA was generated using the full-length zebrafish *vegfc* cDNA sequence cloned into the Gateway pME vector (pDON-221) using Gateway technology (Hartley et al., 2000). For primer sequences, see Supplemental Experimental Procedures. Subsequently a Gateway LR reaction was performed combining a p5E-10xUAS, pME-vegfc and p5E-polyA placing the final 10xUAS:vegfc sequence into pDestTol2pA2AC (containing the α-crystaline promoter driving GFP in the zebrafish lens).

10xUAS:H2AmCherry-IRES-GFPCAAX plasmid DNA was generated by a Gateway LR reaction combining p5E-10xUAS, pME-H2AmCherry and p5E-IRES-GFPCAAX placing the final 10xUAS:H2AmCherry-IRES-GFPCAAX sequence into pDestTol2pA2AC. The pME-H2AmCherry and p3E-IRES-EGFPCAAX were a kind gift from Dr. T. Hall (Parton laboratory, IMB, University of Queensland).

BAC Recombineering

For the generation of *Tg(prox1a:KalTA4)*^{uq3bh} transgenic line, we modified the previously published bacterial artificial chromosome (BAC) plasmid that was used to generate *TgBAC(prox1a:KalTA4-4xUAS-E1b:uncTagRFP)*^{nim5} (Dunworth et al., 2014; van Impel et al., 2014).

Two Tol2 LTRs flanking an ampicillin resistance cassette were placed in the BAC vector backbone using RedET-assisted recombination as previously described (Bussmann and Schulte-Merker, 2011). To remove the expression of 4xUAS:uncTagRFP, the 4xUAS sequence (167 bp) was replaced by a kanamycin resistance cassette using RedET-assisted recombination. The kanamycin cassette was amplified from a pCS2+Citrine plasmid using the following primers: *prox1a* KAN-Forward (*prox1a* BAC homology arm = underlined): 5′-GTTTTTTAATTCGCGGCCGCTCTAGAACTAGTGGATCCCCCGGG CTGCAGCAGCCTGTTGACAATTAATCATCGG-3′; and *prox1a* KAN-Reverse (prox1a BAC homology arm = underlined): 5′-ACTCGCAGATCCGCCAT GGTGGCGGCGAATTCGTGTGGAGGAGCTCAAAGTCAGAAGAACTCGTCA AGAAGGCG-3′.

Embryo Manipulations and Expression Analysis

MO-ccbe1, *MO-vegfr3*, and *MO-vegfc* (Le Guen et al., 2014) and *MO-sox7* and *MO-sox18* (Herpers et al., 2008) were used as previously described. 10xUAS:H2AmCherry-IRES-EGFPCAAX circular DNA (20 ng/μl) and *tol2* transposase mRNA (25 ng/μl) were injected in one-cell-stage embryos. Chemicals were diluted in E3 water with 1% DMSO (Sigma), and embryos were treated from 24 hpf to 3 dpf (for details, see Table S1). FACS analysis (at 30 hpf) was performed as previously described (Kartopawiro et al., 2014). For qRT-PCR primer sequences, see Supplemental Experimental Procedures.

Cellular Transplantation

Transplantation was performed as previously described (Hogan et al., 2009a), with the following changes. Cells from wild-type *Tg(fli1a:nEGFP)* donor embryos were transplanted into wild-type recipients. Embryos with successfully transplanted *Tg(fli1a:n EGFP)* ECs were imaged from 28 hpf to 3 dpf using either a Zeiss LSM 710 FCS confocal microscope or a Zeiss Axiovert 200 spinning disc microscope.

Immunohistochemistry

Immunohistochemistry was performed according to a previously published protocol (Le Guen et al., 2014) with the following modifications. After acetone treatment embryos were treated with Proteinase K at 10 μg/μl diluted in PBS-T. For stage-specific incubation times, see Supplemental Experimental Procedures.

Antibodies used were chicken α-GFP (1:400, Abcam), rabbit α-DsRed (1:400, Living colors, Clontech), rabbit α-Prox1 (1:500, AngioBio Co), and α-rabbit IgG-HRP (1:1,000, Cell Signaling).

Imaging and Quantification

Live and fixed embryos were mounted laterally and imaged using a Zeiss LSM 710 FCS confocal microscope. All images were processed using either ImarisX64 7.70 and/or ImageJ 1.47 (National Institutes of Health, USA) software. Live imaging was performed on laterally mounted embryos imaged above the yolk-extension between somites 8 and 15. For detailed information on quantification methods, see Supplemental Experimental Procedures.

SUPPLEMENTAL INFORMATION

Supplemental Information includes Supplemental Experimental Procedures, four figures, one table, and nine movies and can be found with this article online at http://dx.doi.org/10.1016/j.celrep.2015.10.055.

AUTHOR CONTRIBUTIONS

K.K., A.K.L., and B.M.H. designed, performed, and analyzed experiments and co-wrote the manuscript. C.P.T. designed and performed experiments. E.A.O. and J.C.F. provided unpublished transgenic lines. A.S.Y. and M.F. designed and analyzed experiments.

ACKNOWLEDGMENTS

K.K. was supported by an LE&RN Postdoctoral Fellowship, A.K.L. by a UQ Postdoctoral Fellowship, B.M.H. by an NHMRC/NHF CDF2 (1083811), M.F. by an NHMRC CDF1 (1011242), E.A.O. by the Medical Research Council (U117581329), and A.Y. by an NHMRC Fellowship (1044041). This research was supported by an NHMRC grant (1050138), the ARC project (DP150103110), and the Cariplo Foundation. Imaging was performed in the Australian Cancer Research Foundation's Dynamic Imaging Facility at IMB. We thank M. Affolter, H. Belting, M. Fürthauer, T. Hall, P. Ingham, and J. Bakkers for sharing reagents; S. Paterson and N. Bower for technical assistance; K. Georgas for assistance with schematics; and K. Smith for critical reading of the manuscript.

Received: March 13, 2015
Revised: September 1, 2015
Accepted: October 16, 2015
Published: November 19, 2015

REFERENCES

Bos, F.L., Caunt, M., Peterson-Maduro, J., Planas-Paz, L., Kowalski, J., Karpanen, T., van Impel, A., Tong, R., Ernst, J.A., Korving, J., et al. (2011). CCBE1 is essential for mammalian lymphatic vascular development and

enhances the lymphangiogenic effect of vascular endothelial growth factor-C in vivo. Circ. Res. *109*, 486–491.

Bussmann, J., and Schulte-Merker, S. (2011). Rapid BAC selection for tol2-mediated transgenesis in zebrafish. Development *138*, 4327–4332.

Bussmann, J., Bos, F.L., Urasaki, A., Kawakami, K., Duckers, H.J., and Schulte-Merker, S. (2010). Arteries provide essential guidance cues for lymphatic endothelial cells in the zebrafish trunk. Development *137*, 2653–2657.

Ciruna, B., Weidinger, G., Knaut, H., Thisse, B., Thisse, C., Raz, E., and Schier, A.F. (2002). Production of maternal-zygotic mutant zebrafish by germ-line replacement. Proc. Natl. Acad. Sci. USA *99*, 14919–14924.

Dunworth, W.P., Cardona-Costa, J., Bozkulak, E.C., Kim, J.D., Meadows, S., Fischer, J.C., Wang, Y., Cleaver, O., Qyang, Y., Ober, E.A., and Jin, S.W. (2014). Bone morphogenetic protein 2 signaling negatively modulates lymphatic development in vertebrate embryos. Circ. Res. *114*, 56–66.

François, M., Caprini, A., Hosking, B., Orsenigo, F., Wilhelm, D., Browne, C., Paavonen, K., Karnezis, T., Shayan, R., Downes, M., et al. (2008). Sox18 induces development of the lymphatic vasculature in mice. Nature *456*, 643–647.

Geudens, I., and Gerhardt, H. (2011). Coordinating cell behaviour during blood vessel formation. Development *138*, 4569–4583.

Geudens, I., Herpers, R., Hermans, K., Segura, I., Ruiz de Almodovar, C., Bussmann, J., De Smet, F., Vandevelde, W., Hogan, B.M., Siekmann, A., et al. (2010). Role of delta-like-4/Notch in the formation and wiring of the lymphatic network in zebrafish. Arterioscler. Thromb. Vasc. Biol. *30*, 1695–1702.

Gilbert, S.F. (2000). Principles of experimental embryology. In Developmental Biology, Eighth Edition (Sinauer Associates), pp. 49–76.

Hägerling, R., Pollmann, C., Andreas, M., Schmidt, C., Nurmi, H., Adams, R.H., Alitalo, K., Andresen, V., Schulte-Merker, S., and Kiefer, F. (2013). A novel multistep mechanism for initial lymphangiogenesis in mouse embryos based on ultramicroscopy. EMBO J. *32*, 629–644.

Hartley, J.L., Temple, G.F., and Brasch, M.A. (2000). DNA cloning using in vitro site-specific recombination. Genome Res. *10*, 1788–1795.

Helker, C.S., Schuermann, A., Karpanen, T., Zeuschner, D., Belting, H.G., Affolter, M., Schulte-Merker, S., and Herzog, W. (2013). The zebrafish common cardinal veins develop by a novel mechanism: lumen ensheathment. Development *140*, 2776–2786.

Herpers, R., van de Kamp, E., Duckers, H.J., and Schulte-Merker, S. (2008). Redundant roles for sox7 and sox18 in arteriovenous specification in zebrafish. Circ. Res. *102*, 12–15.

Hirata, J., Nakagoshi, H., Nabeshima, Y., and Matsuzaki, F. (1995). Asymmetric segregation of the homeodomain protein Prospero during Drosophila development. Nature *377*, 627–630.

Hogan, B.M., Bos, F.L., Bussmann, J., Witte, M., Chi, N.C., Duckers, H.J., and Schulte-Merker, S. (2009a). Ccbe1 is required for embryonic lymphangiogenesis and venous sprouting. Nat. Genet. *41*, 396–398.

Hogan, B.M., Herpers, R., Witte, M., Heloterä, H., Alitalo, K., Duckers, H.J., and Schulte-Merker, S. (2009b). Vegfc/Flt4 signalling is suppressed by Dll4 in developing zebrafish intersegmental arteries. Development *136*, 4001–4009.

Hong, Y.K., Harvey, N., Noh, Y.H., Schacht, V., Hirakawa, S., Detmar, M., and Oliver, G. (2002). Prox1 is a master control gene in the program specifying lymphatic endothelial cell fate. Dev. Dyn. *225*, 351–357.

Isogai, S., Hitomi, J., Yaniv, K., and Weinstein, B.M. (2009). Zebrafish as a new animal model to study lymphangiogenesis. Anat. Sci. Int. *84*, 102–111.

Jeltsch, M., Jha, S.K., Tvorogov, D., Anisimov, A., Leppänen, V.M., Holopainen, T., Kivelä, R., Ortega, S., Kärpanen, T., and Alitalo, K. (2014). CCBE1 enhances lymphangiogenesis via A disintegrin and metalloprotease with thrombospondin motifs-3-mediated vascular endothelial growth factor-C activation. Circulation *129*, 1962–1971.

Johnson, N.C., Dillard, M.E., Baluk, P., McDonald, D.M., Harvey, N.L., Frase, S.L., and Oliver, G. (2008). Lymphatic endothelial cell identity is reversible and its maintenance requires Prox1 activity. Genes Dev. *22*, 3282–3291.

Karkkainen, M.J., Haiko, P., Sainio, K., Partanen, J., Taipale, J., Petrova, T.V., Jeltsch, M., Jackson, D.G., Talikka, M., Rauvala, H., et al. (2004). Vascular endothelial growth factor C is required for sprouting of the first lymphatic vessels from embryonic veins. Nat. Immunol. *5*, 74–80.

Kartopawiro, J., Bower, N.I., Karnezis, T., Kazenwadel, J., Betterman, K.L., Lesieur, E., Koltowska, K., Astin, J., Crosier, P., Vermeren, S., et al. (2014). Arap3 is dysregulated in a mouse model of hypotrichosis-lymphedema-telangiectasia and regulates lymphatic vascular development. Hum. Mol. Genet. *23*, 1286–1297.

Kim, H., Nguyen, V.P., Petrova, T.V., Cruz, M., Alitalo, K., and Dumont, D.J. (2010). Embryonic vascular endothelial cells are malleable to reprogramming via Prox1 to a lymphatic gene signature. BMC Dev. Biol. *10*, 72.

Klotz, L., Norman, S., Vieira, J.M., Masters, M., Rohling, M., Dubé, K.N., Bollini, S., Matsuzaki, F., Carr, C.A., and Riley, P.R. (2015). Cardiac lymphatics are heterogeneous in origin and respond to injury. Nature *522*, 62–67.

Kok, F.O., Shin, M., Ni, C.W., Gupta, A., Grosse, A.S., van Impel, A., Kirchmaier, B.C., Peterson-Maduro, J., Kourkoulis, G., Male, I., et al. (2015). Reverse genetic screening reveals poor correlation between morpholino-induced and mutant phenotypes in zebrafish. Dev. Cell *32*, 97–108.

Koltowska, K., Betterman, K.L., Harvey, N.L., and Hogan, B.M. (2013). Getting out and about: the emergence and morphogenesis of the vertebrate lymphatic vasculature. Development *140*, 1857–1870.

Koltowska, K., Paterson, S., Bower, N.I., Baillie, G.J., Lagendijk, A.K., Astin, J.W., Chen, H., Francois, M., Crosier, P.S., Taft, R.J., et al. (2015). mafba is a downstream transcriptional effector of Vegfc signaling essential for embryonic lymphangiogenesis in zebrafish. Genes Dev. *29*, 1618–1630.

Lawson, N.D., and Weinstein, B.M. (2002). In vivo imaging of embryonic vascular development using transgenic zebrafish. Dev. Biol. *248*, 307–318.

Le Guen, L., Karpanen, T., Schulte, D., Harris, N.C., Koltowska, K., Roukens, G., Bower, N.I., van Impel, A., Stacker, S.A., Achen, M.G., et al. (2014). Ccbe1 regulates Vegfc-mediated induction of Vegfr3 signaling during embryonic lymphangiogenesis. Development *141*, 1239–1249.

Mahadevan, A., Welsh, I.C., Sivakumar, A., Gludish, D.W., Shilvock, A.R., Noden, D.M., Huss, D., Lansford, R., and Kurpios, N.A. (2014). The left-right Pitx2 pathway drives organ-specific arterial and lymphatic development in the intestine. Dev. Cell *31*, 690–706.

Martinez-Corral, I., Ulvmar, M.H., Stanczuk, L., Tatin, F., Kizhatil, K., John, S.W., Alitalo, K., Ortega, S., and Makinen, T. (2015). Nonvenous origin of dermal lymphatic vasculature. Circ. Res. *116*, 1649–1654.

Nicenboim, J., Malkinson, G., Lupo, T., Asaf, L., Sela, Y., Mayseless, O., Gibbs-Bar, L., Senderovich, N., Hashimshony, T., Shin, M., et al. (2015). Lymphatic vessels arise from specialized angioblasts within a venous niche. Nature *522*, 56–61.

Okuda, K.S., Astin, J.W., Misa, J.P., Flores, M.V., Crosier, K.E., and Crosier, P.S. (2012). lyve1 expression reveals novel lymphatic vessels and new mechanisms for lymphatic vessel development in zebrafish. Development *139*, 2381–2391.

Pistocchi, A., Bartesaghi, S., Cotelli, F., and Del Giacco, L. (2008a). Identification and expression pattern of zebrafish prox2 during embryonic development. Dev. Dyn. *237*, 3916–3920.

Pistocchi, A., Gaudenzi, G., Carra, S., Bresciani, E., Del Giacco, L., and Cotelli, F. (2008b). Crucial role of zebrafish prox1 in hypothalamic catecholaminergic neurons development. BMC Dev. Biol. *8*, 27.

Sabin, F.R. (1902). On the origin of the lymphatic system from the veins and the development of the lymph hearts and thoracic duct in the pig. Am. J. Anat. *1*, 367–389.

Sauteur, L., Krudewig, A., Herwig, L., Ehrenfeuchter, N., Lenard, A., Affolter, M., and Belting, H.G. (2014). Cdh5/VE-cadherin promotes endothelial cell interface elongation via cortical actin polymerization during angiogenic sprouting. Cell Rep. *9*, 504–513.

Srinivasan, R.S., and Oliver, G. (2011). Prox1 dosage controls the number of lymphatic endothelial cell progenitors and the formation of the lymphovenous valves. Genes Dev. *25*, 2187–2197.

Srinivasan, R.S., Dillard, M.E., Lagutin, O.V., Lin, F.J., Tsai, S., Tsai, M.J., Samokhvalov, I.M., and Oliver, G. (2007). Lineage tracing demonstrates the venous origin of the mammalian lymphatic vasculature. Genes Dev. *21*, 2422–2432.

Srinivasan, R.S., Geng, X., Yang, Y., Wang, Y., Mukatira, S., Studer, M., Porto, M.P., Lagutin, O., and Oliver, G. (2010). The nuclear hormone receptor Coup-TFII is required for the initiation and early maintenance of Prox1 expression in lymphatic endothelial cells. Genes Dev. *24*, 696–707.

Srinivasan, R.S., Escobedo, N., Yang, Y., Interiano, A., Dillard, M.E., Finkelstein, D., Mukatira, S., Gil, H.J., Nurmi, H., Alitalo, K., and Oliver, G. (2014). The Prox1-Vegfr3 feedback loop maintains the identity and the number of lymphatic endothelial cell progenitors. Genes Dev. *28*, 2175–2187.

Stanczuk, L., Martinez-Corral, I., Ulvmar, M.H., Zhang, Y., Laviña, B., Fruttiger, M., Adams, R.H., Saur, D., Betsholtz, C., Ortega, S., et al. (2015). cKit lineage hemogenic endothelium-derived cells contribute to mesenteric lymphatic vessels. Cell Rep. Published online March 10, 2015. http://dx.doi.org/10.1016/j.celrep.2015.02.026.

Tao, S., Witte, M., Bryson-Richardson, R.J., Currie, P.D., Hogan, B.M., and Schulte-Merker, S. (2011). Zebrafish prox1b mutants develop a lymphatic vasculature, and prox1b does not specifically mark lymphatic endothelial cells. PLoS ONE *6*, e28934.

van Impel, A., Zhao, Z., Hermkens, D.M., Roukens, M.G., Fischer, J.C., Peterson-Maduro, J., Duckers, H., Ober, E.A., Ingham, P.W., and Schulte-Merker, S. (2014). Divergence of zebrafish and mouse lymphatic cell fate specification pathways. Development *141*, 1228–1238.

Villefranc, J.A., Nicoli, S., Bentley, K., Jeltsch, M., Zarkada, G., Moore, J.C., Gerhardt, H., Alitalo, K., and Lawson, N.D. (2013). A truncation allele in vascular endothelial growth factor c reveals distinct modes of signaling during lymphatic and vascular development. Development *140*, 1497–1506.

Wigle, J.T., and Oliver, G. (1999). Prox1 function is required for the development of the murine lymphatic system. Cell *98*, 769–778.

Wigle, J.T., Harvey, N., Detmar, M., Lagutina, I., Grosveld, G., Gunn, M.D., Jackson, D.G., and Oliver, G. (2002). An essential role for Prox1 in the induction of the lymphatic endothelial cell phenotype. EMBO J. *21*, 1505–1513.

Yang, Y., García-Verdugo, J.M., Soriano-Navarro, M., Srinivasan, R.S., Scallan, J.P., Singh, M.K., Epstein, J.A., and Oliver, G. (2012). Lymphatic endothelial progenitors bud from the cardinal vein and intersomitic vessels in mammalian embryos. Blood *120*, 2340–2348.

Yaniv, K., Isogai, S., Castranova, D., Dye, L., Hitomi, J., and Weinstein, B.M. (2006). Live imaging of lymphatic development in the zebrafish. Nat. Med. *12*, 711–716.

Yu, F., Kuo, C.T., and Jan, Y.N. (2006). Drosophila neuroblast asymmetric cell division: recent advances and implications for stem cell biology. Neuron *51*, 13–20.